photonics

MDPI

Article

Enhanced Yb:YAG Active Mirrors for High Power Laser Amplifiers

Vladimir A. Petrov [1,2], Gleb V. Kuptsov [1,2], Alyona O. Kuptsova [1,3], Victor V. Atuchin [4,5,6,7,*], Elena V. Stroganova [8] and Victor V. Petrov [1,2,3]

1 Institute of Laser Physics, SB RAS, Novosibirsk 630090, Russia; petrov.nstu@gmail.com (V.A.P.); kuptsov.gleb@gmail.com (G.V.K.); aokupts@gmail.com (A.O.K.); vpetv@laser.nsc.ru (V.V.P.)
2 Faculty of Physical Engineering, Novosibirsk State Technical University, Novosibirsk 630073, Russia
3 Department of Physics, Novosibirsk State University, Novosibirsk 630090, Russia
4 Laboratory of Optical Materials and Structures, Institute of Semiconductor Physics, SB RAS, Novosibirsk 630090, Russia
5 Research and Development Department, Kemerovo State University, Kemerovo 650000, Russia
6 Department of Industrial Machinery Design, Novosibirsk State Technical University, Novosibirsk 630073, Russia
7 R&D Center "Advanced Electronic Technologies", Tomsk State University, Tomsk 634034, Russia
8 Faculty of Physical Engineering, Kuban State University, Krasnodar 350040, Russia; stroganova@kubsu.ru
* Correspondence: atuchin@isp.nsc.ru

Abstract: The work is aimed at the investigation of the influence of nonlinear active ions concentration profiles in Yb:YAG laser elements on temperature distribution and wavefront distortions during amplification using sub-kilowatt level diode pumping. A mathematical model is presented for the theoretical study of the amplification process in crystals with cubic crystal system. A detailed comparison of Yb:YAG active elements with the same thickness and absorbed pumping power, but with various concentration profiles of Yb^{3+}, ions is carried out. It is shown that the use of active elements with an increasing dopant concentration in the pump beam direction allows one to optimize the temperature profile inside the active element and, thus, reduce the thermal-induced wavefront distortions of the amplified radiation. Modeling is carried out for the experimentally grown crystal with linear concentration gradient profile. It is shown that the linear doping profile with a gradient of 0.65 at.%/mm allows increasing the small-signal gain up to 10% and decreasing the thermal-induced wavefront distortions by ~15%.

Keywords: laser materials; ytterbium ions; diode pumping; gradient doping; doping distribution; thermal effects; laser amplifiers; active mirrors; wavefront distortions

Citation: Petrov, V.A.; Kuptsov, G.V.; Kuptsova, A.O.; Atuchin, V.V.; Stroganova, E.V.; Petrov, V.V. Enhanced Yb:YAG Active Mirrors for High Power Laser Amplifiers. *Photonics* **2023**, *10*, 849. https://doi.org/10.3390/photonics10070849

Received: 30 June 2023
Revised: 19 July 2023
Accepted: 20 July 2023
Published: 21 July 2023

1. Introduction

The development of high-intensity laser systems has made it possible to carry out fundamental interdisciplinary research based on the nonlinear interaction of radiation with matter, including such directions as the generation of high-order harmonics [1] and attosecond pulses [2], laser acceleration of charged particles [3], and others [4–7]. Contemporary research in the area of laser technologies is aimed at achieving the high pulse repetition rate required for many applications [8] and at increasing the amplification efficiency in laser amplifiers. Thus, there is a need to create a new element base for high-power laser systems. In particular, one of the important directions of research is the development of active elements with a smoothly varying concentration of dopant ions.

The main motivation for the development of new types of active elements is the optimization of the temperature profile in the active element, which affects both the gain efficiency and the wavefront distortions that occur in the amplified radiation. Wavefront distortions fundamentally limit the energy density in active elements and the minimum achievable diameter of the amplified radiation profile, which reduces the peak power

and intensity [9]. For example, to achieve a 90% efficiency of coherent field combining, the distortion of each field must be less than 1/20 of the wavelength [10]. At present, to solve the problem of a substantially inhomogeneous temperature profile in an active element in high-power laser systems, composite elements consisting of undoped and doped with active ions parts are used. The application of such active elements allows reducing the temperature gradient and increasing the gain coefficient. Such elements are made of crystals [11–13] or ceramics [14].

In conventional active elements with constant doping level, pump radiation is absorbed with exponential decay, which leads to a significant heating of the active element at the pump beam entrance face. This negative effect can be compensated by increasing the concentration of dopant ions along the direction of pump propagation in the active element. As an example, in the case of a ceramic active element, it was shown that when using an active element with several segments with different doping concentrations, a kilowatt-level power can be achieved [15]. However, when ceramics are used, the adding of layers with different doping concentrations can lead to an increase in defects in the active element, which, in turn, leads to a deterioration in the efficiency of generation [16].

Crystalline active elements do not have this drawback. At present, multi-segmented crystalline rods with various concentrations of segments doping with Nd^{3+} ions are widely used [17–21]. In active elements with nonconstant doping, the maximum temperature is lower and the temperature distribution is more uniform than in elements with constant doping. Thus, in such active elements, the mechanical stress induced by the inhomogeneous heating of the active elements is reduced [17,18]. Moreover, experimental studies show that the application of multi-segmented active elements makes it possible to reduce the thermal lens power [18,19]. It is also possible to use active elements consisting of several spatially separated slabs with different doping. This design has been applied in several 100-J level systems [22,23]. The slabs are Yb:YAG ceramics cooled with helium gas.

A promising direction is the application of single-crystal active elements with a gradient profile of dopant ions. In particular, the increased efficiency of such active elements has been experimentally demonstrated for the case of doping with neodymium ions [24–26] and ytterbium ions [27]. As in the case of multi-segmented active elements, gradient doping makes it possible to reduce the temperature gradient in the active element [28], however, multiple interfaces on which optical losses can occur is absent. At present, the growth and application of active elements with gradient doping for high-intensity laser systems are not studied well enough as in growth technologies so in laser physics. Nevertheless, numerous works devoted to reducing the thermal load on active elements in various ways show the relevance of this direction of research.

Ytterbium-doped active elements are widely used in high-intensity laser systems with a high pulse repetition rate [12,22,23,29–32]. High quantum efficiency is an undoubted advantage of ytterbium-doped active media, which makes it possible to reduce the thermal load on active elements. Ytterbium ions are often used as a dopant for such a widespread host material as yttrium aluminum garnet. Garnet crystals form an extensive group of materials with high chemical and mechanical resistance, a wide transparency range, and the possibility of substituting cations to significant dopant concentrations without loss of crystal lattice stability. An important feature of garnets is the absence of anisotropy according to a cubic structure with *Ia*3*d* symmetry, and it significantly reduces the difficulties in growing single crystals of optical quality. At present, garnet crystals are widely used in photonics and laser technologies as matrix materials [33–38]. Garnets possess a cubic crystal structure, but they have a complex arrangement of different cations in the unit cell, and it opens a possibility for changing crystal properties via doping. The wide range of solid solution compositional variation enables the tuning and optimization of optical properties in relation to specific applications.

This work was devoted to studying the influence of active ion concentration nonlinear profiles in Yb:YAG laser elements on the temperature distribution and wavefront distortions of amplified radiation under diode pumping at a sub-kilowatt level. As a first step, a

modelling study was implemented to see the general effects and to estimate the parameters of the optimal gradient distribution of Yb^{3+} ions along the direction of pump radiation. Perspectives of gradiently doped active elements for high-power amplifiers were demonstrated by the study. It was shown that there was a possibility to significantly optimize amplification process using an active element with nonconstant doping distribution. Then, the Yb:YAG crystal with changing Yb^{3+} concentration was grown based on the simulation results. For the grown crystal modeling of temperature distribution, gain and wavefront distortions in the active element, which can be made of the crystal, was carried out.

2. Model and Methods

A three-dimensional non-stationary mathematical model was developed to study the variations of the main physical parameters, as well as the characteristic times of phase and energy changes in radiation parameters occurring as the result of laser amplification process. The model accounts that parameters are distributed over the volume and are in general dependent on time:

$$T = T(x, y, z, t); n_t = n_t(x, y, z); n = n(x, y, z, t), \quad (1)$$

where T—the active element temperature, K; n_t—the concentration of activator ions, cm^{-3}; n—the upper laser level population density, cm^{-3}. The direction along z (longitudinal coordinate) coincides with the beam axis and is along thickness direction of active elements. The zero of the z-axis is at the incident face of the active mirror.

According to the available experimental data for Yb:YAG elements, in the temperature range of 80–300 K emission cross-section at the radiation wavelength (1030 nm) changes by a factor of ~10, the absorption cross-section at the pump wavelength changes by ~2 times, and the thermal conductivity changes by a factor of 5–10 times [39] depending on the degree of doping, the heat capacity is ~5 times [39]. Such changes in the parameters upon transition from cryogenic to room temperature make it necessary to take into account the active element temperature dependencies of the thermophysical and laser parameters. The heat equation thus contains variable coefficients:

$$\rho(T)C(T)\frac{\partial T}{\partial t} = \nabla(\Lambda(T, n_t)\nabla T) - \eta\frac{\partial I_p}{\partial z}, \quad (2)$$

where ρ, C, and Λ—density, g/cm^3, and heat capacity, J/(K·g), and the coefficient of thermal conductivity, W/(cm·K), of the medium, respectively; η—the fraction of absorbed pump radiation power converted to heat; I_p—the intensity of pumping radiation, W/cm^2.

A feature of the model is taking into account the dependence of the thermal conductivity coefficient on temperature and the concentration of doping ions. Based on the analysis of published data [40,41], the dependence of the thermal conductivity coefficient was determined as the function of the temperature and the concentration of optical centers in the YAG:Yb crystal:

$$\Lambda(T, n_t) = A \cdot T + \frac{B - n_t \cdot D}{T} + \frac{E}{T^2 \cdot (F + K \cdot n_t)}, \quad (3)$$

where A, B, D, E, F, and K are constant approximation coefficients. The calculated thermal conductivity coefficient value error is less than 5% compared to published experimental data in the temperature range of 70–330 K.

In this study, a quasi-stationary thermal regime of active elements is considered. It should be mentioned that the quasi-stationary assumption is relevant for amplifiers operating in continuous wave or high pulse repetition rate modes. Despite the quasi-stationary assumption, it is necessary to use a time-dependent model to obtain stabilized temperature distribution.

The system of rate equations account the dependencies of the parameters on temperature:

$$\begin{cases} \frac{\partial I_p}{\partial z} = -\sigma_a(T)\left[(n_t - n) - n \cdot \frac{f_{12}(T)}{f_{01}(T)}\right] I_p \\ \frac{\partial n}{\partial t} = \sigma_a(T)\left[(n_t - n) - n \cdot \frac{f_{12}(T)}{f_{01}(T)}\right] \frac{I_p}{h\nu_p} - n/\tau_L \end{cases}, \quad (4)$$

where σ_a—the absorption cross-section at the wavelength of pumping radiation, cm^2; f_{12} and f_{01}—Boltzmann occupation factors; ν_p—the frequency of pumping radiation, Hz; τ_L—the lifetime of the upper laser level, s.

The Equation (4) is solved jointly with the heat conduction Equation (2). The three-dimensional non-stationary heat conduction equation can be solved by the spatial splitting method on a non-uniform spatial grid. For the heat conduction equation in the simulation, the boundary conditions of the first type on the cooled surface and the second type on all other faces are set. Finally, the small-signal gain is calculated:

$$g(T) = \sigma_L(T)\left[n - (n_t - n) \cdot \frac{f_{01}(T)}{f_{12}(T)}\right], \quad (5)$$

where g—small-signal gain, cm^{-1}; σ_L—the emission cross-section at the wavelength of amplified radiation, cm^2.

Aside the small-signal gain, there is another important characteristic of the amplifier—the magnitude of wavefront distortions introduced into the amplified radiation [42]. Among the main sources of distortions, two main mechanisms can be distinguished: the first arises due to the presence of a temperature gradient in the active element, the second is due to the polarizability change of active ions excited by pump radiation with a nonuniform profile. Both mechanisms lead to a change in the optical path length of individual spatial radiation components in the active element and, as a consequence, to the appearance of an optical path difference between them. The temperature gradient leads to inhomogeneity of the refractive index and the appearance of mechanical stresses. The magnitude of optical path difference associated with the temperature gradient is determined by the relation [43]:

$$\varphi_{\text{th}}(\mathrm{r}, \mathrm{t}) = \left[\frac{dn_0}{dT} + 2 \cdot n_0^3 \cdot \alpha_T \cdot C_r + (n_0 - 1) \cdot (1+\upsilon) \cdot \alpha_T\right] \cdot \int_0^L (T(z, r, t) - T_{bound}) dz, \quad (6)$$

where $\frac{dn_0}{dT}$ is the thermo-optical coefficient of a garnet crystal, K^{-1}; n_0 is the refractive index of the crystal before pumping is turned on; α_T is the coefficient of thermal expansion; C_r is the photoelastic constant; υ is the Poisson's ratio; T_{bound} is the temperature of the cooled face, K; L is the length of the active element, cm.

For a correct comparison of active elements of the same thickness with different doping profiles, it is necessary that the profiles under consideration satisfy the condition of equality of the absorbed pump power:

$$\int_0^L \alpha(z) dz = const, \quad (7)$$

where $\alpha(z)$ is the doping profile of the active element.

Concentration profiles with different growth rates were considered for modeling. The growth rate is limited by the following relation:

$$0 \leq \frac{d}{dz}\alpha(z) \leq G_{max}, \quad (8)$$

where G_{max} is the maximum growth rate of the concentration of activator ions along the length of the crystal, at.%/mm. This relationship takes into account two considerations. Firstly, the concentration of activator ions should increase as pumping propagates in the active element. Secondly, the growth of crystals with a high concentration gradient of the activator imposes significant technological difficulties. In this work, the value of G_{max} = 10 at.%/mm was taken as the maximum rate of increase in the concentration of Yb^{3+} ions.

3. Results

The model was verified by comparison with the experimental results obtained for a cryogenically cooled multidisk laser amplifier with uniformly doped active elements [11,44]. The two-cascade amplifier with a high-power diode pumping was a part of a scalable solid-state laser system targeted to produce pulses with subjoule energy and pulse repetition rate up to 1 kHz. The active elements of this amplifier were diffusion-bonded YAG–Yb:YAG active mirrors. The active mirrors were disk active elements with an antireflection coating on one face and a highly reflective coating on the other. The main advantage of using such elements was the efficient heat dissipation due to the use of the entire area of the highly reflective face as a heat sink.

In addition, when passing through the active mirror, the radiation made a double pass through the amplifying volume (Figure 1), simplifying the optical scheme of the amplifier and reducing its dimensions. Both the doped and undoped parts were disks of 25.4 mm in diameter, and were 3.75 and 2 mm thick, respectively. The active mirrors were cooled using closed-cycle pulse tubes cryocoolers. Such a cooling scheme provided a high operating temperature stability, but the specific feature of closed-loop cryocoolers was the strong nonlinear dependence of the heatsink temperature on the dissipated power. To suppress mechanical vibrations that were produced by operation of pulse tubes, dissected heatsinks with flexible thermal bridges were used [45]. There were eight active elements in the amplifier divided into two stages. The radiation to be amplified made two consecutive round-trips through the first and then through the second amplifier stage. The amplifier was pumped by eight quasi-continuous wave diode lasers with a maximum power of up to 200 W each, central wavelength of 936 nm, and a spectral width of ~10 nm. High average pump power and cryogenic cooling led to strong temperature gradients up to ~50 K/mm [44]. The experimental results and simulated data agreed well; therefore, the model was capable to account complex multielement cooling geometry and nonlinear temperature dependencies of participating parameters.

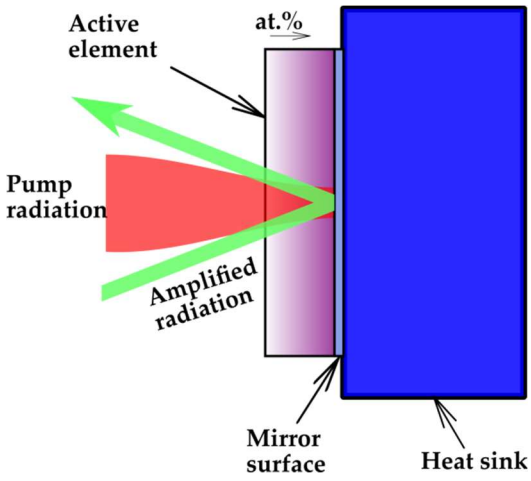

Figure 1. Amplification layout in a gradient doped active mirror.

In this work, the simulation was carried out for gradient doped active mirrors. The following model profiles were chosen: constant, linearly increasing, exponentially increasing reaching a constant value, and hyperbolic (Figure 2). The choice of functions that describe the type of concentration profile was associated, on the one hand, with a qualitative difference between the types of functions, and on the other hand, with the technological possibilities for the growth of such elements. In particular, the hyperbolic profile was interesting because it ensured the uniform absorption of pump radiation and a uniform heat release along the axis of pump radiation [26], reducing element heating.

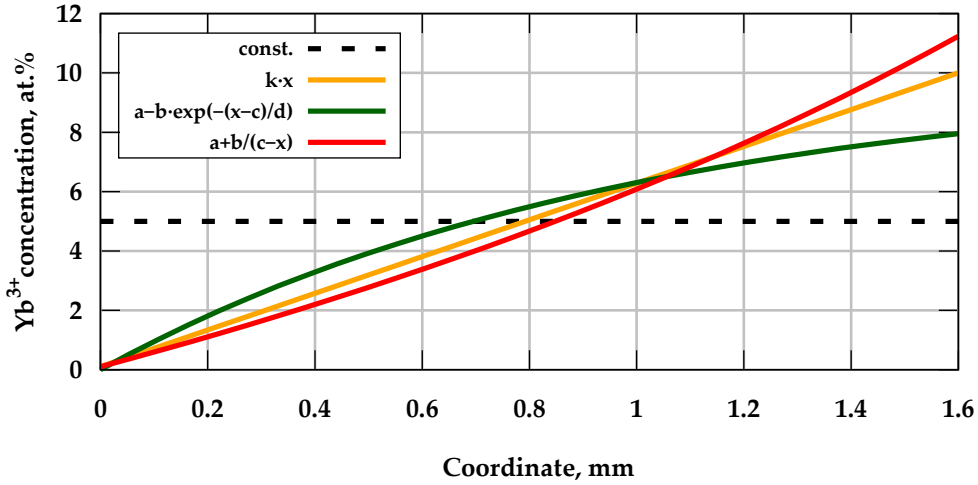

Figure 2. The dependencies of the Yb^{3+} ions concentration on the longitudinal coordinate for various functions of the doping profile.

The coefficients of the functions shown in Figure 2 were chosen so the pump radiation absorption coefficient was ~90% of the incident power for all concentration profiles. It should be noted that a solution of the first equation in (4) included pump radiation reflected from the active mirror surface. Due to the limitation on the maximum value of the activator ion concentration gradient in the crystal, exponential and hyperbolic profiles were close to linear.

The following parameters of pump radiation were used in the simulation: a wavelength of 936 nm, a hyper-Gaussian spatial profile with a diameter of 2 mm ($1/e^2$), and a pump radiation power of 200 W. The center of the profile of the pump radiation spot coincided with the geometric center of the crystal in a plane perpendicular to the longitudinal axis of the pump radiation beam. Figure 3 shows the calculated dependencies of the heating source volumetric power density along the pump radiation axis at the center of the active element:

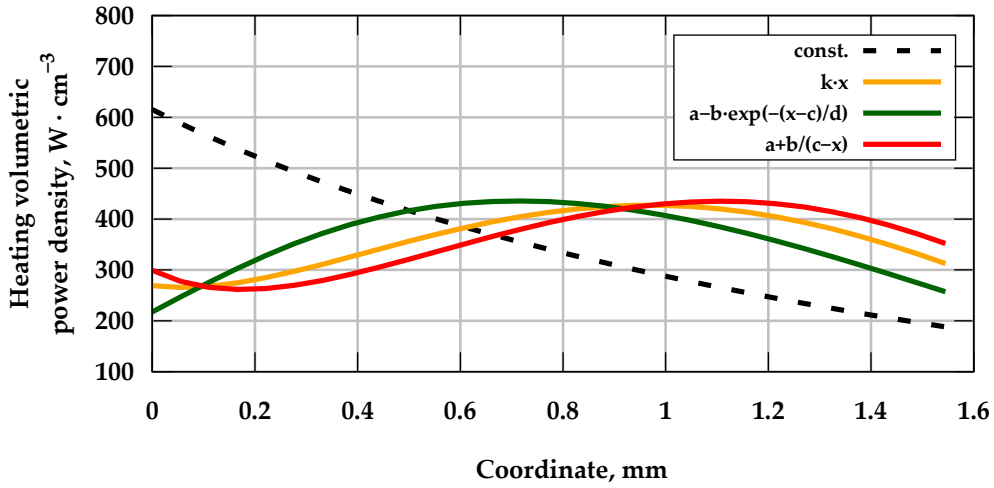

Figure 3. The dependencies of the heating source volumetric power density along the pump radiation axis in the center of the active element.

All profiles with increasing concentration of active ions demonstrated a more uniform heat release with shift of the maximum position closer to the cooled surface and a decrease in the maximum value of the heating source power density by about 30%. The optimization of heat dissipation led to a decrease in the thermal load on the element, and it led to a decrease in the temperature maximum value and gradient. The dependencies of the

temperature at the center of the active element on the coordinate along the pump radiation axis are shown in Figure 4.

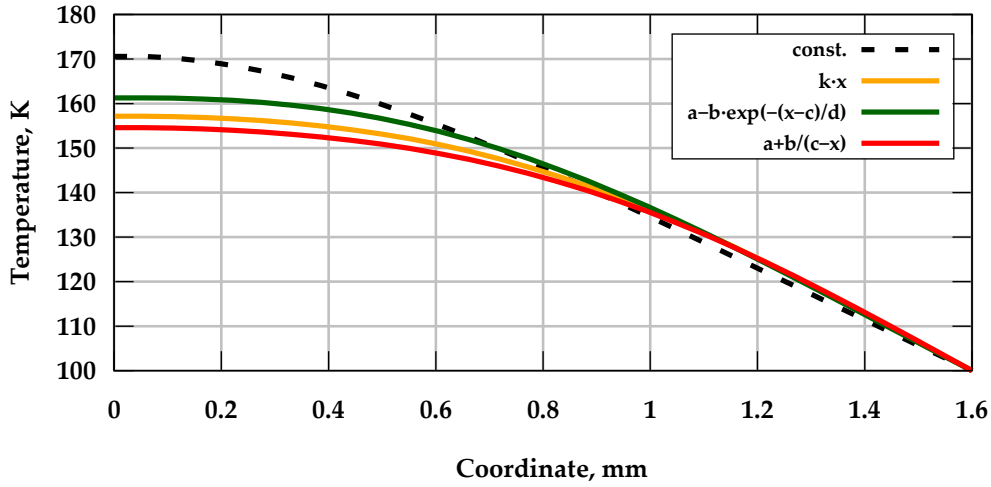

Figure 4. Temperature distribution in the active element along the pump propagation axis for various concentration profiles.

The temperature distributions of different profiles do not differ that much as heating source volumetric power densities, but the change in the optical path length due to temperature changes for the Yb:YAG crystal was equal to ~16.4 nm/(K mm) [41]. The estimated variation in the optical path difference between the constant and hyperbolic profiles was correspondent to a value of about 100 nm (~0.1 wavelength). In addition, the distribution of the stored energy along the active element, which increased towards the cooled face (Figure 5), led to an increase in the gain.

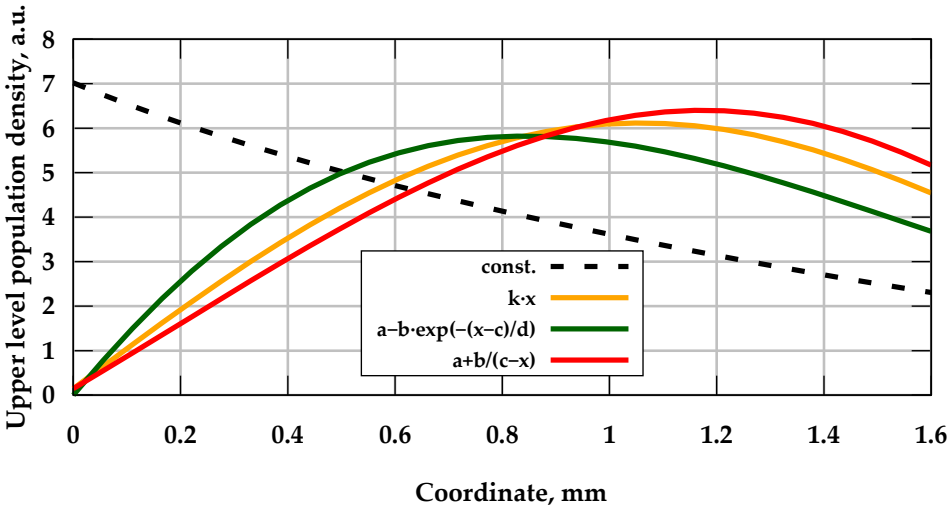

Figure 5. The distribution of upper level population density along the pump radiation axis at the center of the active element.

The distributions of upper level population density were similar to that of the heating source volumetric power density, shifting of the maximum value closer to the cooled surface, thus increasing the gain further. The total gain was: for a constant profile—1.51; for a linear profile—1.64; for an exponential one—1.59; and for a hyperbolic one—1.65. Thus, the increase in the gain was also about 10%.

It followed from the simulation results that the best results, in terms of thermal characteristics and gain, were demonstrated by the hyperbolic profile. However, the difference in results between hyperbolic and linear profiles was relatively small and amounts to

about 1%. The difference in small-signal gain in active elements with linear and hyperbolic profiles was estimated to be less than a percentage. It should be noted that the growth of an active element with a linear Yb^{3+} ions concentration profile seemed to be technologically much simpler than with a hyperbolic one.

Based on the simulation results, an Yb:$Y_3Al_5O_{12}$ crystal was grown [46]. A method for obtaining gradient-activated garnet crystals was developed at Kuban State University [47]. The basis of the technology for obtaining single crystals with a nonlinear controlled distribution of impurity centers was the use of the Czochralski method with melt feeding. The grown crystal is shown in Figure 6.

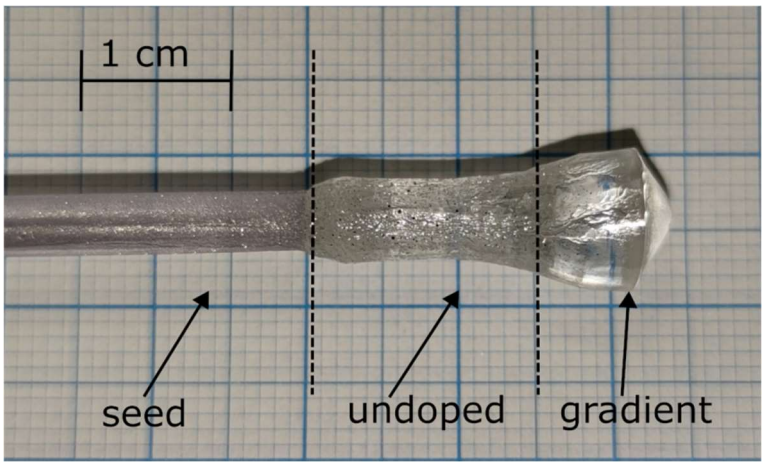

Figure 6. The photograph of the grown Yb:YAG crystal.

The experimental stage of obtaining extreme gradients consisted of an inner crucible and an outer crucible. The inner crucible initially contained no Yb^{3+} ions. The concentration of Yb^{3+} ions was 10 mol.% in the outer one. There was a single short term injection of the melt from the outer crucible to the inner one. The specified diameter of the cylindrical part ("undoped" in Figure 6) was twice the diameter of the seed to mitigate high-speed injection of higher-temperature melt. During the injection, the temperature stabilization was not capable to maintain a constant diameter of the crystal. This was the reason of the presence of bubble defects inside the volume. As shown in Figure 6, the "seed" part was 5 mm wide, the "undoped" part was 7 mm in diameter and 15 mm long, and the "gradient" part was almost 10 mm wide and about 10 mm long. It followed from the spectral characteristics that the integrated absorption in the 850–1060 nm band was increased along the length of the crystal, and it clearly indicated the presence of a concentration gradient of Yb^{3+} optical centers. In Figure 7, the results of spectral-luminescent measurements were shown for the grown crystal gradient section.

As can be seen, despite the target gradient was of the order of 10% at.%/mm, a gradient ~1 at.%/mm was obtained in the experiment. However, 2 sections about 5 mm long could still be used for modeling (Figure 7): linear with a gradient of 0.65 at.%/mm, and an exponential one with a maximum gradient of 1 at.%/mm.

Modeling of the temperature distribution (Figure 8) in a crystal grown with varying concentration according to a linear law with a gradient of 0.65 at.%/mm was carried out in comparison with an Yb:YAG crystal with a fixed concentration of 1.65 at.%, determined from the condition of equal pump absorption in accordance with the formula (7). For the exponential profile, the equivalent value of the constant concentration was 2.1 at.%.

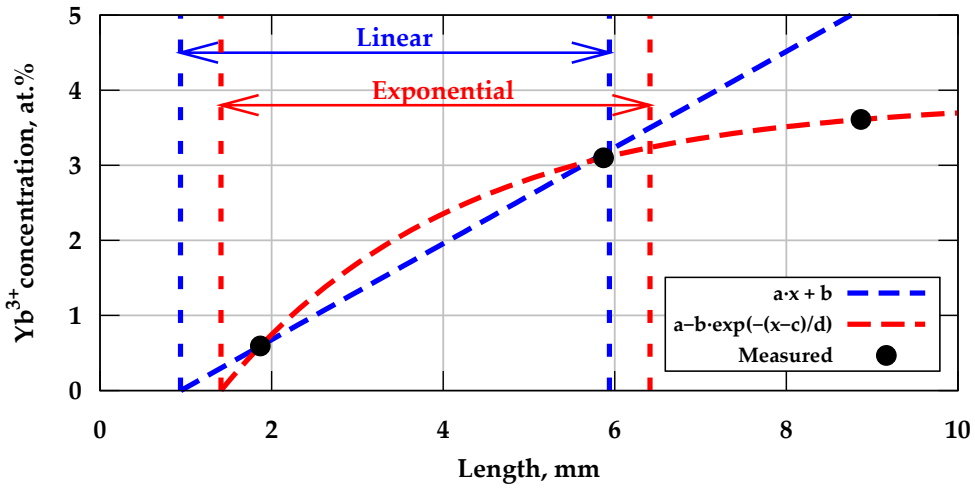

Figure 7. Dependence of the Yb^{3+} ions concentration on the coordinate in the grown crystal.

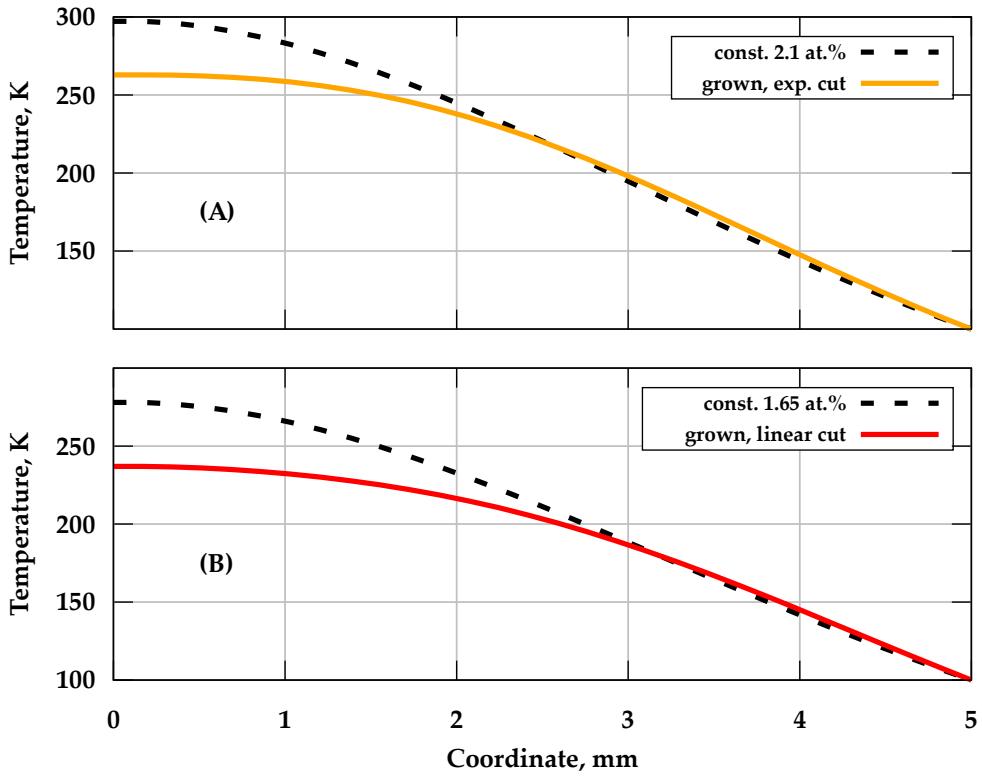

Figure 8. Temperature distribution along the pumping axis for (**A**) exponential and (**B**) linear doping profiles of the grown crystal.

Under these conditions, a temperature difference of ~40 K was observed on the pumping front face in the crystals with constant and linear concentration profiles. As it was seen, the decrease in the maximum temperature value on the front face for the gradient-activated element occured due to the smooth displacement of the main part of the heating source deeper into the element, closer to the cooled surface. The temperature change was about 10% for both cases of exponential and linear profiles. The optical path difference was shorter by ~160 nm (9% shorter) for the exponential profile, and ~250 nm (15% shorter) for the linear profile, both in reference to the corresponding profiles with a constant concentration of active ions.

In Figure 9, the distribution is shown for the population of excited Yb^{3+} laser level over the crystal thickness along the pump axis.

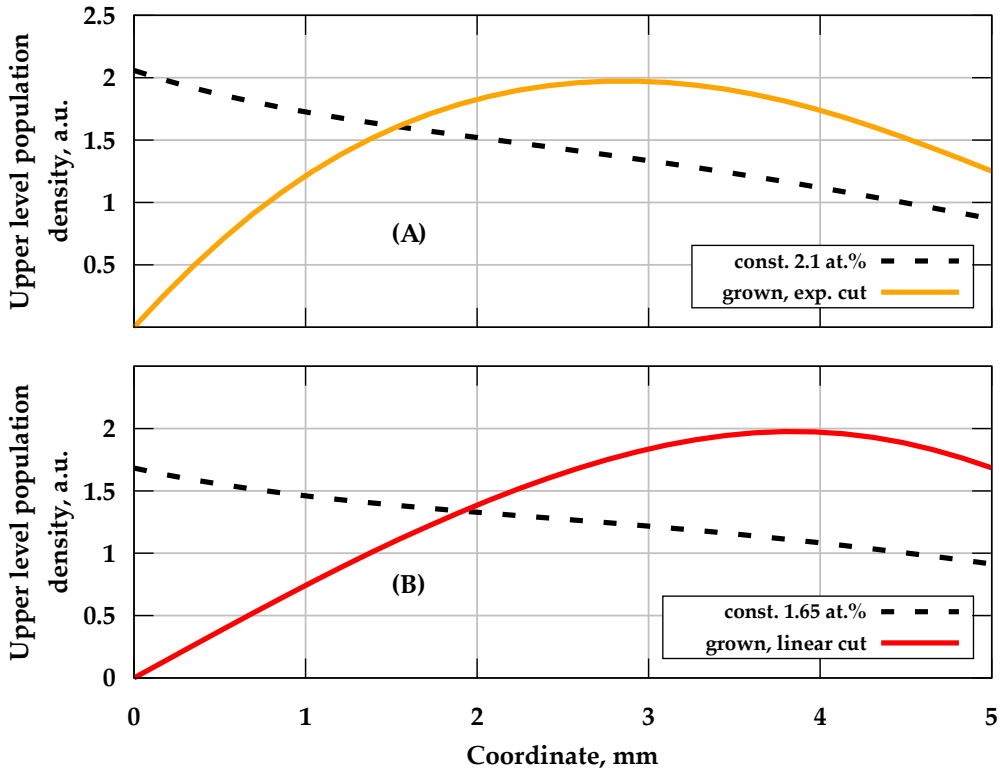

Figure 9. The dependency of the excited Yb^{3+} laser level density on the crystal coordinate for (**A**) exponential and (**B**) linear doping profiles of the grown crystal.

The population dependence of the excited Yb^{3+} laser level on the coordinate had a qualitatively different form for the studied concentration profiles. The linear concentration profile was characterized by a total gain of 1.39, which significantly exceeded the corresponding value of 1.23 for a crystal with a constant activator concentration. For the exponential profile, the gain was 1.33, which also noticeably exceeded the value of 1.21 for a crystal without a gradient.

4. Conclusions

In this work, a detailed comparison was carried out for the disk active elements made of Yb:YAG crystals with the same thickness and absorbed pump power fraction, but with different Yb^{3+} ions concentration profiles along the longitudinal axis. Such profile functions as constant, linear, exponential and hyperbolic were considered in modelling. It was shown that the application of active elements with a concentration gradient of the activator ion in the direction of pump propagation made it possible to optimize the temperature distribution in the active element and, thus, reduce thermally induced wavefront distortions of the amplified radiation. It was shown that the profile given by the hyperbolic function was the most efficient of all the considered gradient profiles.

The presented mathematical model can be used for the theoretical study of the amplification process in different crystals with a cubic crystal system and the search for new promising gradient-doped laser media. It was also possible to calculate optimal gradient doping profiles in a plane perpendicular to the pump radiation axis. The transverse distribution of laser-active ions made it possible to optimize the temperature distributions in active elements cooled from the side faces. Such elements, for example, included rods with end diode pumping. The model can also be further developed to account for the amplified spontaneous emission effect, thickness changes, material anisotropy, heat-induced anisotropy and other effects that were needed to calculate gradient-doped crystals with different crystal systems and pump parameters.

The simulation was also carried out for an experimentally grown crystal with an Yb^{3+} ions concentration gradient. It was shown that the linear doping profile with a gradient of 0.65 at.%/mm made it possible to increase the gain by ~10%, while reducing temperature-induced wavefront distortions by up to ~15%.

Thus, the Yb^{3+} ions concentration gradient at the level of 1 at.%/mm opened a possibility to significantly optimize the amplification process in laser elements in the form of active mirrors. Such an optimization does not require significant redesign of the pumping, cooling systems of a laser system. Generally, an active element can be replaced to a gradiently doped one without any changes in a laser system. The development of crystal growth technology for obtaining concentration gradients of the order of 10 at.%/mm was an important condition for the further optimization of the active element doping profile in order to increase the achievable radiation power of laser systems based on Yb:YAG crystals, while maintaining the quality of the spatial radiation profile.

Author Contributions: Conceptualization, V.A.P. and V.V.P.; data curation, A.O.K. and E.V.S.; investigation, V.A.P., G.V.K. and E.V.S.; methodology, V.V.A. and V.V.P.; resources, E.V.S.; software, V.A.P. and G.V.K.; supervision, V.V.P.; validation, V.V.A.; visualization, G.V.K. and A.O.K.; writing—original draft, V.A.P., G.V.K. and A.O.K.; writing—review & editing, V.V.A. and V.V.P. All authors have read and agreed to the published version of the manuscript.

Funding: The reported study was funded by the Russian Science Foundation grant No. 23-22-00238.

Institutional Review Board Statement: Not applicable.

Informed Consent Statement: Not applicable.

Data Availability Statement: Data are available from the authors on request.

Conflicts of Interest: The authors declare no conflict of interest. The funder had no role in the design of the study; in the collection, analyses, or interpretation of data; in the writing of the manuscript; or in the decision to publish the results.

References

1. Goulielmakis, E.; Brabec, T. High harmonic generation in condensed matter. *Nat. Photonics* **2022**, *16*, 411–421. [CrossRef]
2. Li, J.; Lu, J.; Chew, A.; Han, S.; Li, J.; Wu, Y.; Wang, H.; Ghimire, S.; Chang, Z. Attosecond science based on high harmonic generation from gases and solids. *Nat. Commun.* **2020**, *11*, 2748. [CrossRef] [PubMed]
3. Kim, H.T.; Pathak, V.B.; Hojbota, C.I.; Mirzaie, M.; Pae, K.H.; Kim, C.M.; Yoon, J.W.; Sung, J.H.; Lee, S.K. Multi-GeV Laser Wakefield Electron Acceleration with PW Lasers. *Appl. Sci.* **2021**, *11*, 5831. [CrossRef]
4. Houard, A.; Walch, P.; Produit, T.; Moreno, V.; Mahieu, B.; Sunjerga, A.; Herkommer, C.; Mostajabi, A.; Andral, U.; André, Y.-B.; et al. Laser-guided lightning. *Nat. Photonics* **2023**, *17*, 231–235. [CrossRef] [PubMed]
5. Higginson, A.; Wang, Y.; Chi, H.; Goffin, A.; Larkin, I.; Milchberg, H.M.; Rocca, J.J. Wake dynamics of air filaments generated by high-energy picosecond laser pulses at 1 kHz repetition rate. *Opt. Lett.* **2021**, *46*, 5449–5452. [CrossRef]
6. Smith, D.; Ng, S.H.; Tang, A.; Katkus, T.; Moraru, D.; Juodkazis, S. Crystalline Flat Surface Recovered by High-Temperature Annealing after Laser Ablation. *Photonics* **2023**, *10*, 594. [CrossRef]
7. Emelina, A.; Laryushin, I.; Romanov, A. Dynamics of Gas Ionization by Laser Pulses with Different Envelope Shapes. *Photonics* **2023**, *10*, 499. [CrossRef]
8. Ma, T.; Mariscal, D.; Anirudh, R.; Bremer, T.; Djordjevic, B.Z.; Galvin, T.; Grace, E.; Herriot, S.; Jacobs, S.; Kailkhura, B.; et al. Accelerating the rate of discovery: Toward high-repetition-rate HED science. *Plasma Phys. Control. Fusion* **2021**, *63*, 104003. [CrossRef]
9. Li, J.; Yu, H.; Li, D.; Wang, L.; Zhang, J.; Zhou, Q.; Lv, F.; Lu, X. Influence of Large-Aperture Output Wavefront Distribution on Focal Spot in High-Power Laser Facility. *Photonics* **2023**, *10*, 270. [CrossRef]
10. Bagayev, S.N.; Trunov, V.I.; Pestryakov, E.V.; Leschenko, V.E.; Frolov, S.A.; Vasiliev, V.A. High-intensity femtosecond laser systems based on coherent combining of optical fields. *Opt. Spectrosc.* **2013**, *115*, 311–319. [CrossRef]
11. Kuptsov, G.V.; Petrov, V.A.; Petrov, V.V.; Laptev, A.V.; Konovalova, A.O.; Kirpichnikov, A.V.; Pestryakov, E.V. Laser amplification in an Yb:YAG active mirror with a significant temperature gradient. *Quantum Electron.* **2021**, *51*, 679–682. [CrossRef]
12. Zapata, L.E.; Pergament, M.; Schust, M.; Reuter, S.; Thesinga, J.; Zapata, C.; Kellert, M.; Demirbas, U.; Calendron, A.-L.; Liu, Y.; et al. One-joule 500-Hz cryogenic Yb:YAG laser driver of composite thin-disk design. *Opt. Lett.* **2022**, *47*, 6385–6388. [CrossRef]
13. Al-Hosiny, N.M.; El-Maaref, A.A.; El-Agmy, R.M. Mitigation of Thermal Effects in End Pumping of Nd:YAG and Composite YAG/Nd:YAG Laser Crystals, Modelling and Experiments. *Tech. Phys.* **2021**, *66*, 1341–1347. [CrossRef]

14. Wang, C.; Li, W.; Bai, D.; Zhao, J.; Li, J.; Ba, X.; Ge, L.; Pan, Y.; Zeng, H. Mode-Locked Composite YAG/Yb:YAG Ceramic Laser and High-Power Amplification. *IEEE Photonics Technol. Lett.* **2016**, *28*, 433–436. [CrossRef]
15. Li, M.; Hu, H.; Gao, Q.; Wang, J.; Zhang, J.; Wu, Y.; Zhou, T.; Xu, L.; Tang, C.; Zhao, N.; et al. A 7.08-kW YAG/Nd:YAG/YAG Composite Ceramic Slab Laser with Dual Concentration Doping. *IEEE Photonics J.* **2017**, *9*, 1504010. [CrossRef]
16. Toci, G.; Lapucci, A.; Ciofini, M.; Esposito, L.; Hostaša, J.; Gizzi, L.A.; Labate, L.; Ferrara, P.; Pirri, A.; Vannini, M. Laser and optical properties of Yb:YAG ceramics with layered doping distribution: Design, characterization and evaluation of different production processes. *Proc. SPIE* **2016**, *9726*, 97261P. [CrossRef]
17. Kracht, D.; Wilhelm, R.; Frede, M.; Dupré, K.; Ackermann, L. 407 W End-pumped Multi-segmented Nd:YAG Laser. *Opt. Express* **2005**, *13*, 10140–10144. [CrossRef]
18. Shen, Q.; Cui, X.-Y.; Yan, M.-C.; Eismann, U.; Yuan, T.; Zhang, W.-Z.; Peng, C.-Z.; Chen, Y.-A.; Pan, J.-W. 11-watt single-frequency 1342-nm laser based on multi-segmented Nd:YVO_4 crystal. *Opt. Express* **2019**, *27*, 31913–31925. [CrossRef]
19. Huang, Y.J.; Chen, Y.F. High-power diode-end-pumped laser with multi-segmented Nd-doped yttrium vanadate. *Opt. Express* **2013**, *21*, 16063–16068. [CrossRef]
20. Evangelatos, C.; Tsaknakis, G.; Bakopoulos, P.; Papadopoulos, D.; Avdikos, G.; Papayannis, A.; Tzeremes, G. Actively Q-Switched Multisegmented Nd:YAG Laser Pumped at 885 nm for Remote Sensing. *IEEE Photonics Technol. Lett.* **2014**, *26*, 1890–1893. [CrossRef]
21. Jiang, C.; Huang, W.; He, Q.; He, J.; Zhu, S.; Yin, H.; Li, Z.; Chen, Z.; Dai, S. High-power diode-end-pumped 1314 nm laser based on the multi-segmented Nd:YLF crystal. *Opt. Lett.* **2023**, *48*, 799–802. [CrossRef] [PubMed]
22. Mason, P.D.; Fitton, M.; Lintern, A.; Banerjee, S.; Ertel, K.; Davenne, T.; Hill, J.; Blake, S.P.; Phillips, P.J.; Butcher, T.J.; et al. Scalable design for a high energy cryogenic gas cooled diode pumped laser amplifier. *Appl. Opt.* **2015**, *54*, 4227–4238. [CrossRef]
23. Sekine, T.; Kurita, T.; Hatano, Y.; Muramatsu, Y.; Kurata, M.; Morita, T.; Watari, T.; Iguchi, T.; Yoshimura, R.; Tamaoki, Y.; et al. 253 J at 0.2 Hz, LD pumped cryogenic helium gas cooled Yb:YAG ceramics laser. *Opt. Express* **2022**, *30*, 44385–44394. [CrossRef] [PubMed]
24. Wei, M.-E.; Cheng, T.-Q.; Dou, R.-Q.; Zhang, Q.-L.; Jiang, H.-H. High-peak-power electro-optically Q-switched laser with a gradient-doped Nd:YAG crystal. *Opt. Lett.* **2021**, *46*, 5016–5018. [CrossRef]
25. Botha, R.C.; Koen, W.; Esser, M.J.D.; Bollig, C.; Combrinck, W.L.; von Bergmann, H.M.; Strauss, H.J. High average power Q-switched 1314 nm two-crystal Nd:YLF laser. *Opt. Lett.* **2015**, *40*, 495–497. [CrossRef]
26. Wilhelm, R.; Freiburg, D.; Frede, M.; Kracht, D. End-pumped Nd:YAG laser with a longitudinal hyperbolic dopant concentration profile. *Opt. Express* **2008**, *16*, 20106–20116. [CrossRef]
27. Azrakantsyan, M.; Albach, D.; Ananyan, N.; Gevorgyan, V.; Chanteloup, J.-C. Yb^{3+}:YAG crystal growth with controlled doping distribution. *Opt. Mater. Express* **2012**, *2*, 20–30. [CrossRef]
28. Wei, M.; Cheng, T.; Dou, R.; Zhang, Q.; Jiang, H. Superior performance of a 2 kHz pulse Nd:YAG laser based on a gradient-doped crystal. *Photonics Res.* **2021**, *9*, 1191–1196. [CrossRef]
29. Wang, Y.; Chi, H.; Baumgarten, C.; Dehne, K.; Meadows, A.R.; Davenport, A.; Murray, G.; Reagan, B.A.; Menoni, C.S.; Rocca, J.J. 1.1 J Yb:YAG picosecond laser at 1 kHz repetition rate. *Opt. Lett.* **2020**, *45*, 6615–6618. [CrossRef]
30. Herkommer, C.; Krötz, P.; Jung, R.; Klingebiel, S.; Wandt, C.; Bessing, R.; Walch, P.; Produit, T.; Michel, K.; Bauer, D.; et al. Ultrafast thin-disk multipass amplifier with 720 mJ operating at kilohertz repetition rate for applications in atmospheric research. *Opt. Express* **2020**, *28*, 30164–30173. [CrossRef]
31. Nubbemeyer, T.; Kaumanns, M.; Ueffing, M.; Gorjan, M.; Alismail, A.; Fattahi, H.; Brons, J.; Pronin, O.; Barros, H.G.; Major, Z.; et al. 1 kW, 200 mJ picosecond thin-disk laser system. *Opt. Lett.* **2017**, *42*, 1381–1384. [CrossRef]
32. Ogino, J.; Tokita, S.; Kitajima, S.; Yoshida, H.; Li, Z.; Motokoshi, S.; Morio, N.; Tsubakimoto, K.; Fujioka, K.; Kodama, R.; et al. 10-J, 100-Hz conduction-cooled active-mirror laser. *Opt. Contin.* **2022**, *1*, 1270–1277. [CrossRef]
33. Atuchin, V.V.; Beisel, N.F.; Galashov, E.N.; Mandrik, E.M.; Molokeev, M.S.; Yelisseyev, A.P.; Yusuf, A.A.; Xia, Z. Pressure-stimulated synthesis and luminescence properties of microcrystalline $(Lu,Y)_3Al_5O_{12}:Ce^{3+}$ garnet phosphors. *ACS Appl. Mater. Interfaces* **2015**, *7*, 26235–26243. [CrossRef]
34. Ji, H.; Wang, L.; Molokeev, M.S.; Hirosaki, N.; Xie, R.; Huang, Z.; Xia, Z.; ten Kate, O.M.; Liu, L.; Atuchin, V.V. Structure evolution and photoluminescence of $Lu_3(Al,Mg)_2(Al,Si)_3O_{12}:Ce^{3+}$ phosphors: New yellow-color converters for blue LED-driven solid state lighting. *J. Mater. Chem. C* **2016**, *4*, 6855–6863. [CrossRef]
35. Galashov, E.N.; Atuchin, V.V.; Gavrilova, T.A.; Korolkov, I.V.; Mandrik, Y.M.; Yelisseyev, A.P.; Xia, Z. Synthesis of $Y_3Al_5O_{12}:Ce^{3+}$ phosphor in the Y_2O_3–Al metal–CeO_2 ternary system. *J. Mater. Sci.* **2017**, *52*, 13033–13039. [CrossRef]
36. Slimi, S.; Jambunathan, V.; Pan, M.; Wang, Y.; Chen, W.; Loiko, P.; Solé, R.M.; Aguiló, M.; Díaz, F.; Smrz, M.; et al. Cryogenic laser operation of a "mixed" Yb:LuYAG garnet crystal. *Appl. Phys. B* **2023**, *129*, 57. [CrossRef]
37. Vistorskaja, D.; Laurikenas, A.; Montejo de Luna, A.; Zarkov, A.; Pazylbek, S.; Kareiva, A. Sol-Gel Synthesis and Characterization of Novel $Y_{3-x}M_xAl_{5-y}V_yO_{12}$ (M—Na, K) Garnet-Type Compounds. *Inorganics* **2023**, *11*, 58. [CrossRef]
38. Dubov, V.; Gogoleva, M.; Saifutyarov, R.; Kucherov, O.; Korzhik, M.; Kuznetsova, D.; Komendo, I.; Sokolov, P. Micro-Nonuniformity of the Luminescence Parameters in Compositionally Disordered GYAGG:Ce Ceramics. *Photonics* **2023**, *10*, 54. [CrossRef]
39. Sui, Y.; Yuan, M.; Bai, Z.; Fan, Z. Recent Development of High-Energy Short-Pulse Lasers with Cryogenically Cooled Yb:YAG. *Appl. Sci.* **2022**, *12*, 3711. [CrossRef]

40. Dong, J.; Bass, M.; Mao, Y.; Deng, P.; Gan, F. Dependence of the Yb^{3+} emission cross section and lifetime on temperature and concentration in yttrium aluminum garnet. *J. Opt. Soc. Am. B* **2003**, *20*, 1975–1979. [CrossRef]
41. Aggarwal, R.L.; Ripin, D.J.; Ochoa, J.R.; Fan, T.Y. Measurement of thermo-optic properties of $Y_3Al_5O_{12}$, $Lu_3Al_5O_{12}$, $YAlO_3$, $LiYF_4$, $LiLuF_4$, BaY_2F_8, $KGd(WO_4)_2$, and $KY(WO_4)_2$ laser crystals in the 80–300 K temperature range. *J. Appl. Phys.* **2005**, *98*, 103514. [CrossRef]
42. Tamer, I.; Keppler, S.; Hornung, M.; Körner, J.; Hein, J.; Kaluza, M.C. Spatio-Temporal Characterization of Pump-Induced Wavefront Aberrations in Yb^{3+}-Doped Materials. *Laser Photonics Rev.* **2018**, *12*, 1700211. [CrossRef]
43. Antipov, O.L.; Anashkina, E.A.; Fedorova, K.A. Electronic and thermal lensing in diode end-pumped Yb:YAG laser rods and discs. *Quantum Electron.* **2009**, *39*, 1131–1136. [CrossRef]
44. Kuptsov, G.V.; Konovalova, A.O.; Petrov, V.A.; Laptev, A.V.; Atuchin, V.V.; Petrov, V.V. Laser Method for Studying Temperature Distribution within Yb:YAG Active Elements. *Photonics* **2022**, *9*, 805. [CrossRef]
45. Petrov, V.V.; Kuptsov, G.V.; Petrov, V.A.; Laptev, A.V.; Kirpichnikov, A.V.; Pestryakov, E.V. Optimisation of a multidisc cryogenic amplifier for a high-intensity, high-repetition-rate laser system. *Quantum Electron.* **2018**, *48*, 358–362. [CrossRef]
46. Petrov, V.A.; Kuptsov, G.V.; Petrov, V.V.; Laptev, A.V.; Stroganova, E.V. Development of laser elements with non-linear distribution of active ions. In Proceedings of the 2022 International Conference Laser Optics (ICLO), St. Petersburg, Russia, 20–24 June 2022. [CrossRef]
47. Galutskiy, V.V.; Vatlina, M.I.; Stroganova, E.V. Growth of single crystal with a gradient of concentration of impurities by the Czochralski method using additional liquid charging. *J. Cryst. Growth* **2009**, *311*, 1190–1194. [CrossRef]